Ultrathin Polymer Films with Intrinsic Microporosity: Anomalous Solvent Permeation and High Flux Membranes

*Patricia Gorgojo, Santanu Karan, Him Cheng Wong, Maria F. Jimenez-Solomon, João T Cabral, and Andrew G. Livingston**

Organic solvent nanofiltration (OSN) membranes with ultrathin separation layers down to 35 nm in thickness fabricated from a polymer of intrinsic microporosity (PIM-1) are presented. These membranes exhibit exceptionally fast permeation of n-heptane with a rejection for hexaphenylbenzene of about 90%. A 35 nm thick PIM-1 membrane possesses a Young's modulus of 222 MPa, and shows excellent stability under hydraulic pressures of up to 15 bar in OSN. A maximum permeance for n-heptane of 18 $Lm^{-2}h^{-1}bar^{-1}$ is achieved with a 140 nm thick membrane, which is about two orders of magnitude higher than Starmem240 (a commercial polyimide-based OSN membrane). Unexpectedly, decreasing the film thickness below 140 nm results in an anomalous decrease in permeance, which appears to be related to a packing enhancement of PIM-1, as measured by light interferometry. Further, thermal annealing of the membranes formed from PIM-1 reveals that their permeance is preserved up to temperatures in excess of 150 °C, whereas the permeance of conventional, integrally skinned, asymmetric polyimide OSN membranes decreases significantly when they are annealed under the same conditions. To rationalize this key difference in response of functional performance to annealing, the concept of membranes with intrinsic microporosity (MIMs) versus membranes with extrinsic microporosity (MEMs) is introduced.

1. Introduction

Many of the conventional separation and purification processes in oil and gas, chemical, and pharmaceutical industries utilise large amounts of organic solvents and entail high energy consumption.[1] Such processes could be totally or partially replaced by membrane technology, with an order of magnitude lower energy consumption. To enable this, membranes need to be both chemically resistant to the solvents involved and provide high flux, in order to process large solvent volumes with a viable area and in a viable timeframe.

Dr. P. Gorgojo, Dr. S. Karan, Dr. H. C. Wong, Dr. M. F. Jimenez-Solomon, Dr. J. T. Cabral, Prof. A. G. Livingston
Department of Chemical Engineering
Imperial College London, Exhibition Road
South Kensington Campus
London, SW7 2AZ, UK
E-mail: a.livingston@imperial.ac.uk

DOI: 10.1002/adfm.201400400

Existing state of the art polymeric membranes are either integrally skinned asymmetric (ISA) or thin film composite (TFC) membranes.[2] ISA membranes are produced by the phase inversion technique which leads to a dense separation layer a few hundred nanometres thick being formed on a highly porous support structure several microns in thickness. Of the ISA membranes, crosslinked polyimide (PI) membranes are probably the most widely used for OSN due to their ease of fabrication, high mechanical strength, and high stability even in harsh solvents such as tetrahydrofuran or dimethylformamide.[3–5] However, physical aging and compaction remains a challenge for ISA membranes, resulting in permeance reduction over time in operation, often by more than 50% in a few days.[6] Studies show that the intrinsic solvent permeance of ISA membranes formed from polyimide is negligible; solvent cast or annealed films of polyimide, in which the polymer chain conformation relaxes to pack closer to equilibirum, typically have low or no flux.[4] The permeance difference between polyimide ISA membranes and dense polyimide films arises because ISA membranes formed by phase inversion rapidly "freeze" the polyimide microporous structure, which can be far away from equilibrium; importantly, the resulting microporosity is due to the way the membrane is made. Under service conditions, or when the membranes are heated and then cooled gradually ("annealed"), these membranes age (lose permeance) as the polymer chains relax towards equilibrium packing.

TFC membranes are typically fabricated by depositing or forming a thin separation layer on top of a porous ultrafiltration (UF) support several microns thick.[7,8] These membranes are attracting widespread interest for OSN because the separation layer structure can be better controlled and, therefore, the separation performance improved.[6] Crucially, when the top layer is formed by coating of rubbery polymers[7] or by interfacial polymerisation,[8] both resulting in crosslinked matrices, there is less evidence of physical aging or compaction. However, fluxes of ISA and most TFC membranes are still relatively low and large membrane areas are necessary for industrial applications. Recently, the preparation of ultrathin (35 – 50 nm) free-standing

diamond-like carbon (DLC) nanosheet membranes has been reported.[9] These DLC membranes can retain organic dyes (182.2–562.7 g.mol^{-1}) at permeances three orders of magnitude higher than those of commercially available ISA membranes, due to their rigid hydrophobic pores of ≈ 1 nm, which allow the ultrafast viscous permeation of organic solvents. While the scale-up of this approach for application is challenging, it shows what can be achieved with nano-scale engineering approaches, and directs research to consider how to prepare ultrathin separation layers with higher permeance and better selectivity from polymers.[9]

Techniques such as dip or flow coating,[7,10] interfacial polymerization,[11] and spin casting,[12] are candidates for the fabrication of thin selective films on polymer supports for OSN.[7,8,13] Polymers of intrinsic microporosity (PIMs) have received a great deal of attention as a separating layer material for TFC membranes to be used for gas separations[14–18] and pervaporation applications.[19,20] PIMs are defined as polymers providing a continuous network of interconnected intermolecular voids, which forms as a direct consequence of the shape and rigidity of the component macromolecules.[21] Therefore, PIMs-based membranes are expected to exhibit high permeance and selectivity, which makes them a promising material for OSN. Fritsch and co-workers[22] produced PIM-1 TFC membranes for OSN by dip-coating a solution of PIM-1 onto a PAN support, resulting in a film exhibiting 30 times higher n-heptane permeance than Starmem240 (a polyimide-based OSN membrane from Grace Davison Membranes), without signs of aging or compaction of the PIM-1 layer.[22] Tsarkov and co-workers[23] used PIM-1 for OSN with different dyes in ethanol, and reported significant sorption of the dyes within the membrane. Based on these previously reported high solvent permeances, PIM-1 emerges as an attractive material to use for fabrication of ultrathin films, which we expect will have outstanding OSN permeation properties. Moreover, since PIM-1 is a polymer of intrinsic microporosity, we anticipate that if the membrane is fabricated so that the polymer is closer to an equilibrium state, there should not be noticeable effects of annealing on the membrane permeance; that is, we expect that the resulting membrane will exhibit intrinsic microporosity.

Here, we present the preparation and OSN performance of ultrathin PIM-1 films. These films were prepared via spin coating and the effect of thickness on their OSN performance was studied. Membranes were fabricated by transferring the PIM-1 films with thicknesses in the range of 35–660 nm onto UF supports, and were successfully employed for molecular separation of hexaphenylbenzene (HPB) from heptane solution. For comparison purposes, a 30 µm thick self-standing PIM-1 membrane was produced from slow solvent evaporation from a petri dish containing PIM-1 solution in chloroform. All membranes showed approximately 90% rejection of HPB. The nature of the membrane microporosity, i.e. membranes of intrinsic microporosity versus membranes of extrinsic microporosity (MIMs versus MEMs), was explored by subjecting these PIM films to prolonged heating at a designated temperature. Pre- and post-annealing results from the PIM-1 membranes are compared with the permeance values obtained for ISA polyimide (Matrimid) membranes, which we also prepared for this work by the phase inversion method.

2. Results and Discussion

We prepared PIM-1 films of varying thickness via spin coating of PIM-1 chloroform solutions of different concentrations (0.25–2.5 wt.%) onto glass or silicon wafers (100). The thin films were then floated and made free-standing in DI water, and finally transferred onto either a polyacrylonitrile (PAN) UF support or an alumina support (150 nm pore size). The fabrication steps are summarized in **Figure 1**. The average molecular weight (M_n) and polydispersity index of PIM-1 was determined via gel permeation chromatography (GPC); a M_n of 99 200 g.mol^{-1} and a polydispersity of 1.8 were obtained.

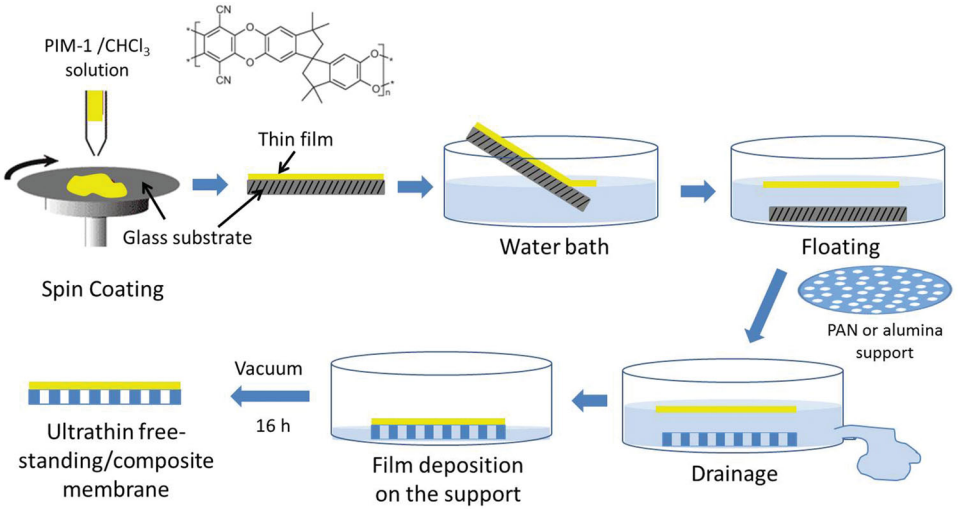

Figure 1. Schematic of the preparation process for ultrathin PIM-1 membranes via spin coating on glass and transfer to a porous support (polyacrylonitrile (PAN) or anodised alumina). Concentrations of PIM-1 in chloroform ($CHCl_3$) used for spin coating were in the range from 0.25 to 2.5 wt.% (w/w).

Table 1. N_2 adsorption/desorption analysis of PIM-1 powder and a free-standing 1 µm PIM-1 membrane

Sample name	Annealing Temperature [°C][a)]	BET surface area [m^2 g^{-1}]	t-Plot micropore area [m^2 g^{-1}]
PIM-1 polymer powder	50	777	270
	100	792	281
	200	767	288
1 µm PIM-1 membrane	50	671	-
	100	811	293
	200	774	317

[a)]Annealing under N_2 flow.

2.1. Characterization of PIM-1 Membranes

2.1.1. N_2 Adsorption/Desorption

Low temperature N_2 adsorption measurements revealed values of areas from Brunauer–Emmett–Teller (BET) analysis for PIM-1 powder in the range 700–900 m^2 g^{-1} (see **Table 1**) which are in good agreement with values reported in the literature.[14] It is well established that the microporosity in PIM-1 films is due to the presence of free volume elements of effective size below 2 nm which are created during film formation, or precipitation from solution.[17] PIM-1 molecules are inflexible due to the absence of single bonds in the backbone, but contorted due to the presence of spiro-centres (see Figure 1). Table 1 shows that the values obtained for the polymer powder do not change as the degasification temperature increases. On the other hand, the BET surface area of a 1 µm free-standing membrane degassed at 50 °C shows an initial value below 700 m^2 g^{-1} which increases up to 800 m^2 g^{-1} as the degassing temperature reaches 100 °C. This may be due to incomplete desorption of moisture and remaining solvent, i.e. chloroform from the casting solution, which remain in the membrane at low temperature. BET isotherms of both samples, PIM-1 powder and the 1 µm free-standing PIM-1 membrane, are shown in Figure S1a.

2.1.2. Differential Scanning Calorimetry (DSC) and Thermogravimetric Analysis (TGA)

DSC analyses revealed no glass transition temperature (T_g) for PIM-1 powder or the 1 µm free-standing PIM-1 membrane up to 450 °C, in agreement with data from the literature.[18,20,24] PIM-1 is amorphous and remains glassy up to its decomposition temperature, which was >350 °C as confirmed via TGA analysis. The TGA spectrum of PIM-1 is shown in Figure S1b.

2.1.3. Thickness Calibration

Thicknesses of PIM-1 films deposited on polymeric porous supports were determined by scanning electron microscopy (SEM). Images in **Figure 2** correspond to PIM-1 membranes prepared via spin coating of solutions with polymer concentrations between 0.25 and 2.5 wt.%. The thinnest membrane spun cast was 35 nm thick (Figure 2a and d) and the thickest one was 660 nm thick (Figure 2f). Glass substrates were found to be the best option for the spin coating process, as the PIM-1 films could be easily detached by immersing in a water bath. Atomic force microscopy (AFM) and SEM images of the PAN support are shown in Figure S2. The surface roughness of the support was calculated as the root mean square (RMS) roughness from AFM data and a value of 3.5 nm was obtained. This low value indicates rather smooth surfaces, suitable for support of ultrathin films. As inferred from the SEM images, a good adherence was observed between PIM-1 films and PAN substrates after the drying process. Under same conditions, PIM-1 solutions were also spin coated on silicon wafers for interferometry and AFM characterization. Figure 2c depicts

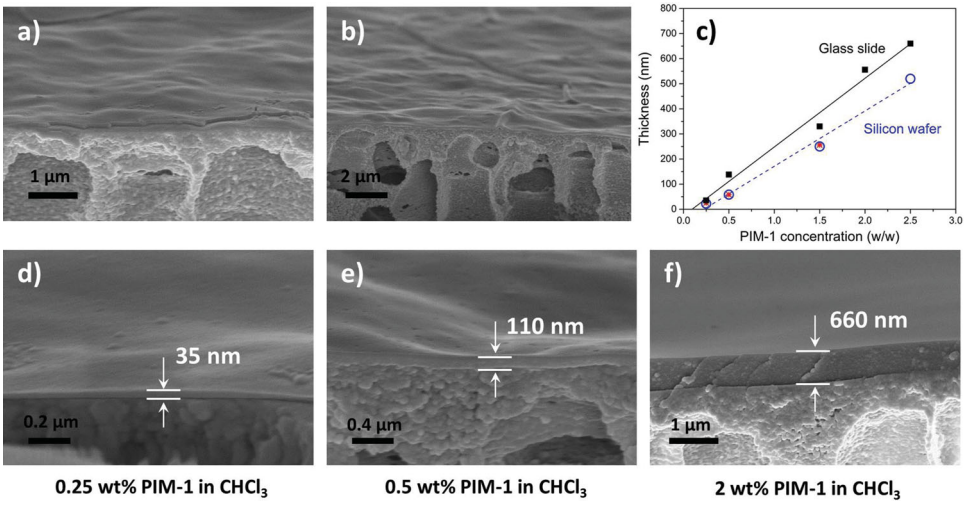

Figure 2. SEM images of ultrathin PIM-1 membranes at different magnifications on porous PAN support. Thin films were prepared on a glass plate via spin coating a solution of PIM-1 with different polymer concentrations in chloroform and then transferred to PAN supports. (a,d) 0.25 wt.%; (b,e) 0.5 wt.%; (f) 2.5 wt.%. c) Film thickness dependence on PIM-1 solution concentration and (■) glass and (○,*) silicon substrates, spin coated at 2000 rpm. Thickness values were obtained by scanning electron microscopy (SEM, ■), atomic force microscopy (AFM, ○) and light interferometry (*).

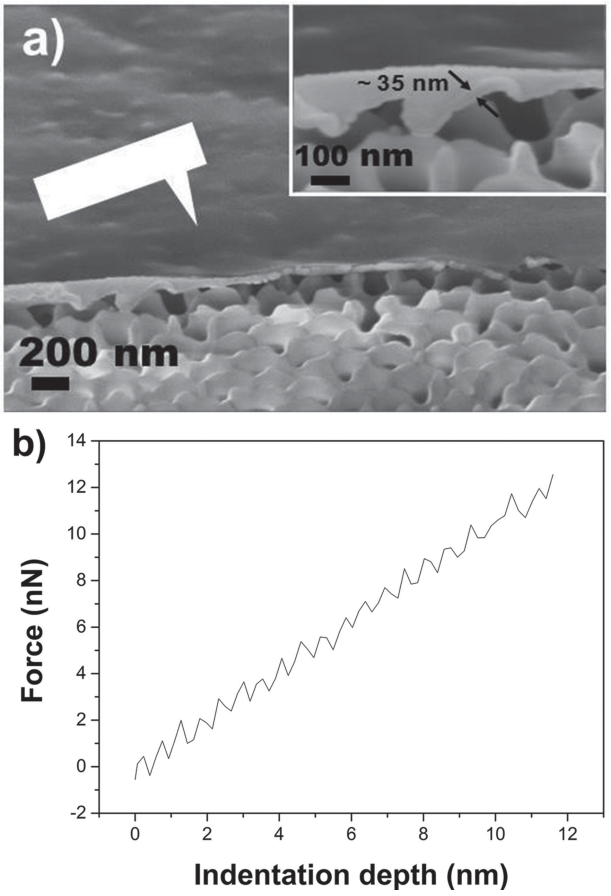

Figure 3. (a) SEM image of a 35 nm PIM-1 film on a 150 nm pore size alumina support. Inset on top is a higher magnification image of the same membrane, and: (b) indentation curve obtained from AFM to calculate the Young's modulus value for a 35 nm thick film.

the thickness of the PIM-1 film as determined by SEM, AFM, and interferometry versus the polymer concentration in solution (0.25 to 2.5 wt.% (w/w)). 2.5 wt.% PIM-1 solutions spun on glass gave rise to PIM-1 films of 660 nm in thickness. Glass and silicon substrates gave slightly different thickness due to the differences in surface tension between the fluid and the surfaces of the substrates.

2.1.4. Mechanical Properties via Atomic Force Microscopy (AFM)

To investigate the mechanical toughness of the ultrathin PIM-1 films, they were transferred onto the alumina supports to obtain free standing sections, whose mechanical response is not convoluted with that of the substrate. **Figure 3**a shows the SEM image of a 35 nm thick film produced from a 0.25 wt% (w/w) PIM-1 solution, which was used to determine the mechanical properties of these films. Figure 3b depicts the indentation plot used to measure the Young's modulus for a 35 nm thick film.

To avoid the alumina substrate affecting the results, the AFM tip was placed on the free-standing film on the top of the centre of a pore. The Young's modulus value was measured from fitting of the indentation curve using JPK data processing software employing a quadratic pyramid tip shape. A Young's modulus of 222 ± 35 MPa was obtained. A thicker PIM-1 film (660 nm) on alumina gave a value of 242 ± 35 MPa. Song and co-workers.[25] determined the overall Young's modulus of pristine PIM-1 film with thickness of 1μm and obtained a value of 6.94 GPa and a hardness of 0.23 GPa. Thus, our results indicate that the free-standing PIM-1 films (35 – 660 nm thick) formed via spin coating produced much softer films compared to the rigid pristine PIM-1 film with 1μm thickness.

2.2. Nanofiltration by Ultrathin PIM-1 Membranes

The fabrication steps, especially the floating and transfer of the ultrathin films to the support membranes, are somewhat challenging and can lead to defects. For instance, the film may tear apart, or wrinkles can form if water is trapped in between the support and the membrane. In addition, the drying step is crucial: evaporation of water from inside the PAN support has to be as slow as possible in order to obtain good adhesion between the PIM-1 film and the PAN support, and defect free films. This process takes approximately 16–24 h.

The permeance of the PAN UF support was obtained for heptane and HPB-heptane solutions at pressures of 13, 20, and 30 bar. Irreversible decay of solvent flux with pressure was observed for pure heptane, from 632.5 $Lm^{-2}h^{-1}bar^{-1}$ at 13 bar down to 170.7 $Lm^{-2}h^{-1}bar^{-1}$ at 30 bar after three consecutive filtrations of pure heptane, HPB-heptane solution and back again to pure heptane (see Figure S3 and Table S1). Heptane permeances for UF PAN supports at 13 bar (pressure set for nanofiltration of PIM-1 membranes) were in all cases higher than 600 $Lm^{-2}h^{-1}bar^{-1}$.

For the OSN membranes, filtrations were carried out using pure heptane and heptane solutions containing HPB or polystyrene oligomer standards (PS) at 13–15 bar pressure and 30 °C temperature. The rejection of HPB was in the range of 86–90%, as calculated from the absorbance at 248 nm in UV. **Figure 4** shows the UV spectra of the feed, permeate and retentate solutions of (a) a 35 nm thick membrane, and; (b) a 660 nm thick membrane. It is clear that HPB molecules are not adsorbed in the membrane as the HPB concentration of the retentate increases in comparison with the feed concentration.

Nanofiltration of PS-heptane solution was also carried out in a cross flow system to confirm the reproducibility and demonstrate the ultrathin PIM-1 membranes long time performance (up to 168 h). Molecular weight cut-off (MWCO) curves using PS oligomers for 35 nm thick PIM-1 membranes are shown in Figure S4 in both dead end cell and cross flow filtration systems. Heptane permeance values were similar whether the filtration was carried out with pure heptane, heptane-HPB or heptane-PS, suggesting that there is no concentration polarization effect as the feed concentrations are quite low (0.5 g L^{-1} for PS and 10 mg L^{-1} for HPB).

For industrial applications, permeance, also referred to as pressure-normalized flux, is a key parameter to evaluate any process in economic terms. High flux is desirable and, for a specific polymer membrane system, can be achieved via different strategies: increasing the pressure, increasing the membrane area, or for example by reducing the thickness of

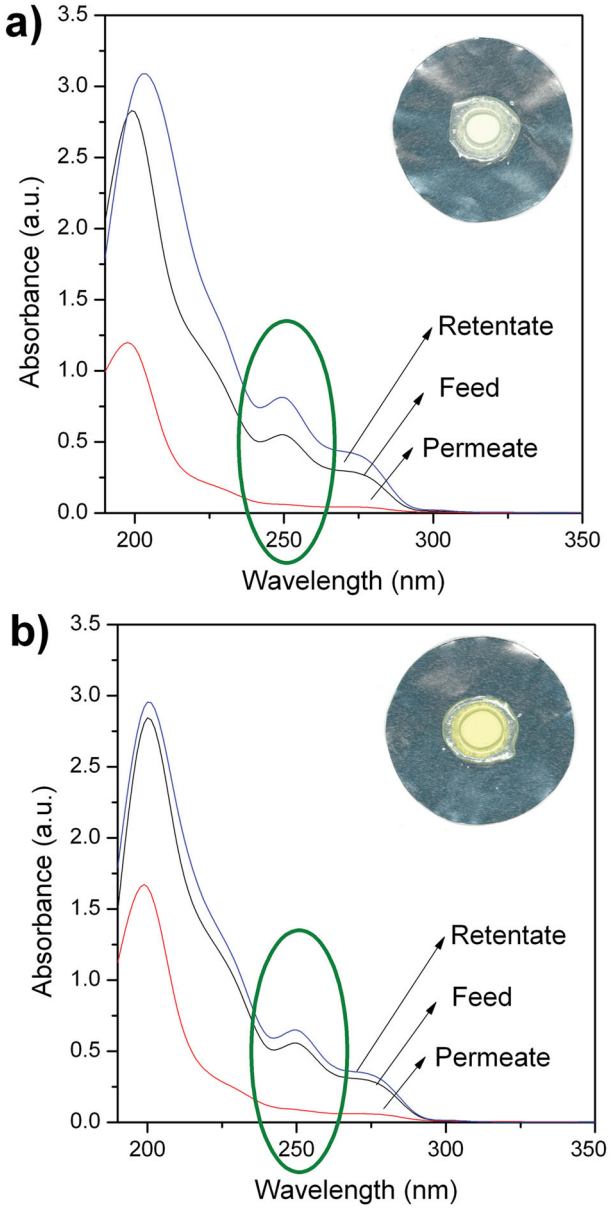

Figure 4. UV absorbance spectra (200–350 nm) of feed, permeate and retentate solutions from the filtration of HPB-n-heptane solution through (a) a 35 nm thick, and (b) a 660 nm thick membrane. Top right hand side shows pictures of membranes mounted on aluminium foil and sealed by means of solvent resistant resin. The diameter of the aluminium disc is 5 cm and the effective area of the membranes is between 0.78 and 1.5 cm^2.

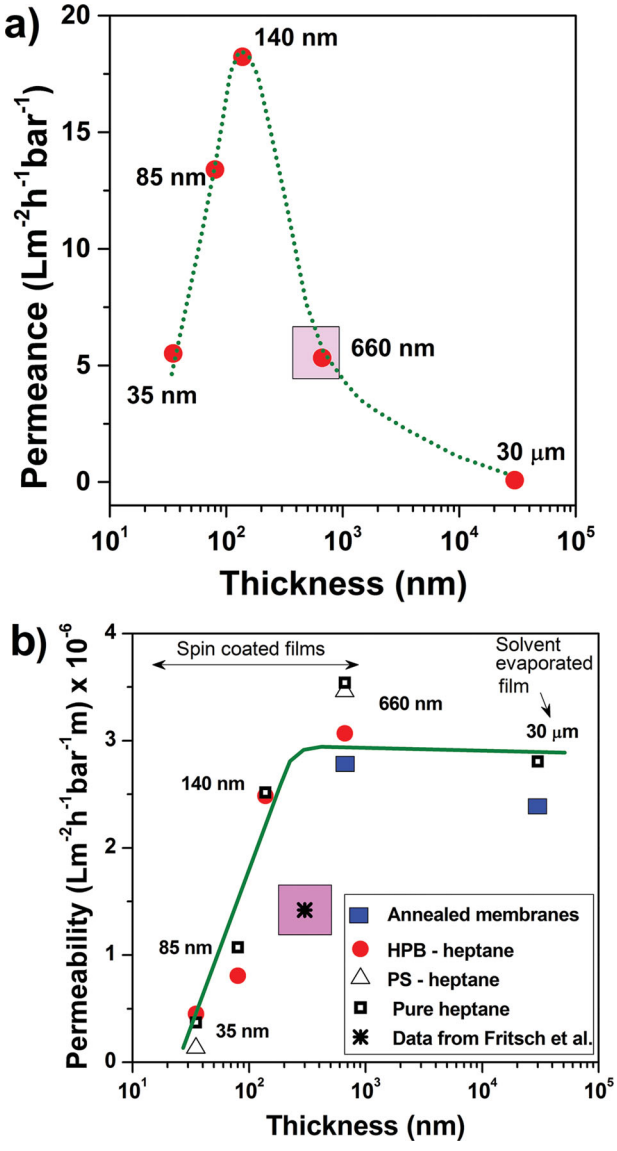

Figure 5. (a) Permeance and (b) permeability versus thickness for ultrathin PIM-1 membranes supported on PAN and thick free-standing PIM-1 membranes. Filtrations of pure heptane and HPB/heptane solutions were carried out at 13 bar and 30 °C in a dead end cell system and filtrations of styrene oligomers/heptane solutions were performed at 15 bar and 30 °C in a cross flow system. The pink boxes between 300–700 nm represent values obtained by Fritch and co-workers.[22]

the selective layer in composite membranes. **Figure 5**a shows heptane permeance values versus thickness of prepared PIM-1 membranes. A maximum value of 18 $Lm^{-2}h^{-1}bar^{-1}$ was obtained for a 140 nm thick PIM-1 membrane. By decreasing the thickness of the selective layer we were trivially expecting to achieve higher permeance, conditional to mechanical stability of the film, and this was indeed observed initially as thickness decreased from approximately 1 µm. However, below 140 nm a gradual decrease in permeance with decreasing thickness was found. This unexpected decrease in permeance for the thinnest membranes might be explained by a decrease in free volume due to structural relaxation of the films as they become thinner. This phenomenon has been extensively studied in flexible polymers,[26,27] but has not yet been reported for PIMs. This data therefore shows that fabricating a very thin selective layer may not always offer higher solvent permeance. It is challenging to analyse the physical behaviour of polymer thin films when the thickness of the film is few tens of nanometers. Ultrathin polymer films generally exhibit lower glass transition temperatures and faster ageing, depending on the confining surface interactions, and so reducing the thickness could cause a decrease in the intrinsic porosity when compared to the bulk polymer. In contrast, published work on ultrathin diamond-like

carbon (DLC) membranes.[9] shows that their permeance is extremely high and is preserved at such small thicknesses because of the rigid cross-linked structure of the amorphous carbon.

To elucidate the nature of this anomalous behavior, permeances were normalized with thickness to obtain permeability values ($Lm^{-1}h^{-1}bar^{-1}$). Permeability is commonly used for dense membranes in gas separation and is defined as permeance multiplied by thickness. Therefore, it is an intrinsic property independent of thickness, which indicates the ability of the material to allow molecules to pass through. In Figure 5b, the permeability of heptane is plotted against thickness (from 35 nm thin film composite to 30 µm free standing membranes) and it is evident that permeability of the PIM-1 films is constant above thicknesses of approximately 100 nm; below this, thinner films become less permeable. Table S2 in the supporting information shows the permeance and permeability data for PIM-1 membranes from 35 to 660 nm thick. To investigate this proposed structural relaxation, measurements of film thickness during a temperature scan from room temperature up to 450 °C were performed. **Figure 6**a depicts film thickness versus annealing temperature for PIM-1 films spun on silicon substrates. Generally, the thin films were spun and dried at ambient conditions before testing, yielding thicknesses of 22 nm, 58 nm and 263 nm. An additional film with comparable thickness of the intermediate 58 nm film, viz. 65 nm, was extensively dried under vacuum for one week. The results are qualitatively unchanged, and ambient drying conditions are most relevant for practical membrane applications. Larger excess free volumes are observed for thicker films, whereas thinner films relax less in both absolute (as expected) and relative terms. Results normalised by the initial thickness (Figure 6b) show negligible change in thickness up to 150 °C, after which the films slowly reduce in thickness up to 350 °C. At temperatures above 350 °C we noticed a steeper thickness decrease, which is likely due to thermal degradation.[20] These results agree qualitatively with membrane performance data; confined thin films with lower T_g are expected to pack more efficiently, as they are closer to equilibrium, and thus exhibit lower permeability. The resulting non-linear dependence of membrane permeance with thickness appears to be related to a non-monotonic packing upon film confinement. It is known that thin film confinement alters the packing of glass forming liquids, including polymers.[26–29] Changes occur for thicknesses typically <100 nm for flexible polymers.[28,29] Intensive properties such as mechanical properties and the glass transition temperature become extensive, i.e. thickness dependent, and dependent on interaction with the substrate. In general, as polymer films become thinner, they become 'softer', with lower T_g, and pack more effectively.[30] Thin film membranes are expected to behave similarly, albeit the exact thickness at which the intrinsic-extrinsic transition occurs will depend on chain stiffness or persistence length, which are expected to be relatively large for PIM-1.

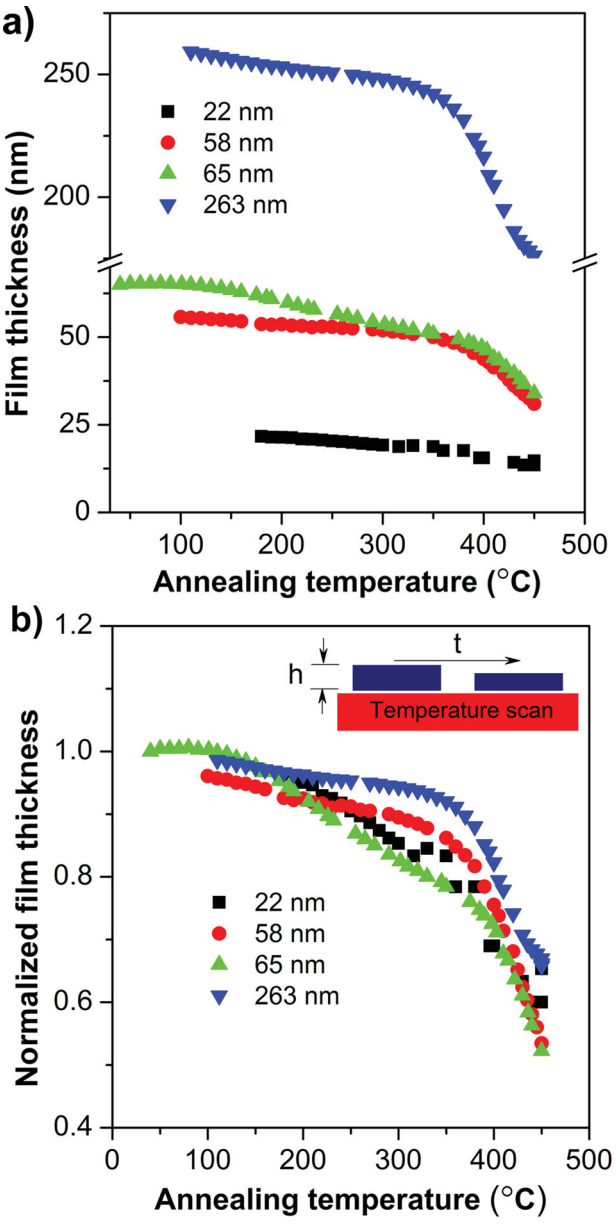

Figure 6. (a) Film thickness (h), and (b) normalised thickness of PIM-1 films spun on silicon substrates obtained by interferometry measurements at annealing temperature from 30 to 450 °C.

2.3. Intrinsic and Extrinsic Microporosity in Polymeric Membranes

In conventional integrally skinned asymmetric membranes, the microporosity is extrinsic and arises from the templating effects of solvent molecules and chain conformation in the dope solution at the onset of phase inversion. This "extrinsic" microporosity can be lost when the polymer rearranges over time or due to an applied pressure or high temperature.[6,31] See-Toh et al.[31] showed that heating P84 polyimide ISA membranes up to 200 °C and then cooling them to ambient temperature caused the microporosity to collapse and the flux to reduce to zero. In this work, Matrimid polyimide ISA membranes were prepared on non-woven supports via phase inversion and the membranes obtained were annealed by heating at 50, 100, 150 and 200 °C prior to cooling to ambient temperature. Permeance of heptane decreased from 1.01 L m^{-2} h^{-1} bar^{-1} for the non-annealed membrane down to 0.058 $Lm^{-2}h^{-1}bar^{-1}$ for the membrane annealed at 150 °C, and no flux was observed after annealing at 200 °C (**Table 2**).

Table 2. Permeance values of integrally skinned asymmetric matrimid polyimide (PI) membranes obtained for pure n-heptane in a dead end cell (DEC). Membranes were annealed for 2 h at each temperature. Ultrathin PIM-1 films supported on alumina were annealed at 150 °C for 2 h.

Membrane	Annealing temperature [°C] (2 h)	Permeance of pure heptane [L m^{-2} h^{-1} bar^{-1}]
Asymmetric membrane from matrimid	Nil	1.0
	50	0.6
	100	0.3
	150	0.06
	200	0
Self-standing PIM-1 film (30 µm thick)	Nil	0.09
	100	0.09
	150	0.08
600 nm thick PIM-1 film on PAN	Nil	4.6[a)]
600 nm thick PIM-1 film on alumina	150	4.5[a)]

[a)]Permeance of heptane containing HPB (10 mg mL^{-1})

The effect of annealing was also investigated for the 30 µm PIM-1 dense membranes produced by solvent-evaporation in petri dishes. Data for these membranes, presented in Table 2, shows that heptane permeance for the membrane annealed at 150 °C for 2 h is still close to that of the un-annealed membrane. However, it is likely that the actual separating layer in the Matrimid PI ISA membrane is of the order of <1000 nm, representing a fraction of the overall membrane thickness, and so one might expect this to undergo more rapid permeance loss than a 30 micron thick film. To make a more relevant comparison, a composite membrane with a PIM-1 layer thickness of 600 nm on an alumina support (see Figure S5) was annealed at 150 °C for 2 h. The annealed PIM-1 film showed a very similar solvent permeance (close to 5 $Lm^{-2}h^{-1}bar^{-1}$) to the unannealed PIM-1 membrane supported on PAN (Table 2). This result suggests that the properties of PIM-1 in films with thicknesses down to few hundreds of nanometers remain the same under annealing, i.e., are intrinsic to the membrane. However, recent studies of physical aging in glassy polymer film membranes have revealed that the aging behaviour in confinement does differ from that in bulk.[12] Paul and co-workers.[12] have investigated the properties of films formed from glassy polymers as thin as 20 nm for gas separation, and reported accelerated ageing kinetics compared to thicker films. It has also been found that free-standing polysulfone (PSF) thin films exhibit accelerated aging relative to bulk PSF, with aging rates that strongly depend on film thickness.[32,33] Murphy et al.[34] studied the aging of thin PSF layers confined in multilayered structures, and concluded that the aging rate is similar to bulk PSF.[34], thereby supporting the idea that accelerated aging in thin films is due to the presence of interfaces, rather than geometric confinement.

3. Conclusion

Ultrathin polymer membranes have been fabricated using PIM-1 and successfully applied to organic solvent nanofiltration, with rejection of HPB of about 90% in heptane. PIM-1 membranes of 600 nm to 30 µm thick were annealed up to 150 °C and showed no decrease in permeance; therefore it is confirmed that microporosity is preserved in such films, i.e. these are membranes with intrinsic microporosity (MIMs). By contrast, integrally skinned asymmetric matrimid polyimide membranes fabricated by the phase-inversion method lost permeance upon annealing. This result indicates that their microporosity is extrinsic, i.e. they are membranes with extrinsic microporosity or MEMs. A maximum permeance value for heptane of 18 $Lm^{-2}h^{-1}bar^{-1}$ was achieved with a 140 nm thick PIM-1 membrane, which is 90 times higher permeance than the commercial benchmark Starmem240 (a polyimide based OSN membrane from Grace Davison Membranes). Its mechanical response was found to be robust to nanofiltration pressures of ca 10 bar. The performance of even thinner membranes deteriorated, which is interpreted as due to enhanced packing upon further confinement. Compared to diamond-like carbon membranes,[9] the ultrathin PIM-1 polymer membranes have the advantages of low cost, flexibility and simple fabrication process.

4. Experimental Section

Materials: Polymer of intrinsic microporosity PIM-1 was kindly supplied by Evonik Membrane Extraction Technology, UK. Matrimid was kindly supplied by Huntsman Corporation. Polyacrylonitrile (PAN), average Mw 150 000, Hexaphenylbenzene (HPB, 98% Mw 534.6 g mol^{-1}) and sodium metabisulphite were purchased from Sigma Aldrich, UK, and used as received. Non-woven polypropylene fabric was purchased from Novatex, Germany, (product code 2471). HPLC grade DMF, chloroform and heptane were purchased from VWR international. The polystyrene oligomers for MWCO evaluation were purchased from Varian Ltd, UK. Alumina supports were purchased from Synkera Technologies, Inc., US. Silicon wafers (100) were purchased from Compart Technology Ltd, UK.

Characterization of PIM-1: Gel permeation chromatography (GPC) analyses were performed to determine the molecular weight and polydispersity of PIM-1. The GPC system was equipped with an Agilent refractive index detector and THF was used as the mobile phase at a flow rate of 1 mL min^{-1}. It was run at a temperature of 40 °C with a Waters HT3 column calibrated using polystyrene also at 40 °C. Differential scanning calorimetry (DSC) experiments were carried out using a TA Instruments Q2000 autosampler system equipped with a nitrogen cooling system and TzeroTM technology to improve baseline flatness and stability. DSC measurements were performed under a helium environment and temperature and heat capacity were calibrated using a sapphire standard. The glass transition temperature T_g and heat capacity step ΔCp of 'fresh' glasses were computed from the second heating run at 10 °C min^{-1}, following the onset/mid-point criterion (intersection between the glass and midpoint tangents). Thermogravimetric analyses were performed with a TGA Q500 by TA Instruments, UK. Nitrogen adsorption measurements were performed with a TriStar surface area analyzer (Micrometrics). PIM-1 powder was degassed at 50 °C under N_2 flow for 12 h before the analysis. The same sample was subsequently degassed at 100 and 200 °C also for 12 h and N_2 adsorption measurements were performed.

Preparation of Porous Polyacrylonitrile (PAN) Support Membrane: Support membranes were prepared from PAN via phase inversion. PAN powder

was dissolved as received at room temperature in a mixture of DMF and DI water (11 wt.% polymer/ 86 wt.% DMF/ 3 wt.% H_2O) by means of mechanical stirring until an homogeneous solution was obtained and left overnight to allow the removal of air bubbles before its use. Membranes were cast on non-woven polypropylene fabric using the prepared dope solution on a continuous casting machine with the adjustable knife set at 200 µm and a speed of 0.035 m s^{-1}. Immediately after casting, the membrane was immersed in a water bath (22 °C) where phase inversion occurred. After 10 min, membranes were transferred twice to fresh water baths and were finally stored in a 1 wt.% Sodium metabisulphite solution.

Ultrathin and Free-Standing PIM-1 Membrane Preparation: PIM-1 was dissolved in chloroform ($CHCl_3$) at different concentrations: 0.25, 0.5, 1.5, 2.0, and 2.5 wt.%. These solutions were filtered through a PTFE syringe filter (0.45 µm pore size) and spin coated on glass slides at 2000 rpm and 20 °C. Films were floated on water and deposited on PAN or alumina supports and annealed in a vacuum oven at 25 °C as depicted in Figure 1. 30 µm free standing PIM-1 membranes were prepared as follows: 1 wt.% polymer solution was prepared in $CHCl_3$, and then filtered through a 0.45 µm PTFE syringe filter and subsequently cast on a Petri dish. The solvent evaporated at room temperature and the obtained film was detached from the glass.

Integrally Skinned Asymmetric Matrimid Polyimide (PI) Nanofiltration Membranes: ISA PI membranes were prepared by the phase-inversion method. Solutions of 22 wt.% of Matrimid (2:1 wt.% of NMP:THF) were cast on a glass plate using an Elcometer machine with the knife set at a thickness of 300 µm. Immediately after casting, the membranes were immersed in a water bath at 23 °C.

Membrane Characterization: Ultrathin PIM-1 membranes were characterized by scanning electron microscopy with a high resolution field emission gun scanning electron microscope (Carl Zeiss Ltd.) operating at 5 kV. Samples were coated with chromium with a sputtered current of 75 mA for 2 min (Emitech K575X Sputter Coater, Quorum Technologies Ltd.) under an argon atmosphere to achieve the necessary conductivity. For the analysis of cross sections, samples were freeze-fractured in liquid nitrogen and coated.

The evolution of film thickness as a function of temperature was determined using a modified UV-vis interferometer (Filmetrics F20-UV). In order to conduct interferometry measurements, PIM-1 thin films were prepared on silicon wafers via spin coating. Thin films were annealed using a Linkam heating stage (THMS600) at the rate of 10 °C per min, while film thicknesses were measured and analyzed with FilmMeasure data analysis software.

The surface topographies of the PIM-1 as cast thin films were characterized by atomic force microscopy (Innova, Bruker AXS) in tapping-mode, using phosphorous doped Si tips (RTESPW, Bruker). Scanning was performed at a speed of 0.5 Hz, and a scan size of 5 µm. A sampling resolution of 512 points per line was selected. Surface roughness is obtained as root-mean-square (RMS) roughness (Rq), average roughness (Ra), or peak-to-valley height (Rz) using SPMLabAnalysis (V 7.00) analysis software.

Surfaces of PAN supports were analysed via AFM on a Veeco AFM Dimension 3100 equipped with a DAFMLN Dimension AFM Scan Head and a Nanoscope VI controller. Samples were attached to glass slides using a double sided tape. The scans were performed in an air medium. The images were scanned in tapping mode using silicon cantilevers having a nominal diameter of less than 10 nm. Scanning was performed at a speed of 1.3 Hz, and a scan size of 1 µm was used for standard images. A sampling resolution of 512 points per line was selected.

A JPK Nanowizard Atomic Force Microscope was used to determine the elasticity modulus of different thickness PIM-1 films at RT (22 °C). The probe was a Bruker's Sharp Microlever (MSNL-10) using tip E with a quadratic pyramid shape, a spring constant of 0.1714 N m^{-1} and a sensitivity value of 29.7 nm V^{-1}.

N_2 adsorption measurements were also carried out to determine BET surface area and micropore area of the 30 µm dense membranes prepared by solvent evaporation.

Organic Solvent Nanofiltration Performance: Filtrations were carried out using pure heptane and heptane solutions containing hexaphenylbenzene (HPB) or polystyrene standards (PS) at 13–15 bar and 30 °C. A stirred dead end cell system was used for the filtration of pure solvent and heptanes-HPB solutions. A cross flow system was used on selected membranes for long term experiments up to 168 h. Pieces of the ultrathin PIM-1 membranes supported on PAN were sandwiched between two pieces of aluminium tape and sealed with epoxy resin. The membranes had an effective area in the range of 0.78–1.5 cm^2. The concentrations of the feed solutions were 0.01 g L^{-1} of HPB in heptane and 0.5 g L^{-1} of PS in heptane. Solvent flux (J) was determined by measuring permeate volume (V) per unit area (A) per unit time (t) according to Equation (1). The rejection (R_i) of HPB and PS was calculated from Equation (2), where $C_{P,i}$ and $C_{F,i}$ correspond to concentrations of solutes in the permeate and the feed respectively.

$$J = \frac{V}{A \cdot t} \tag{1}$$

$$R_i = \left(1 - \frac{C_{P,i}}{C_{F,i}}\right) \cdot 100\% \tag{2}$$

HPB concentrations in the feed, retentate and permeate were analysed by UV-vis spectrometry. UV spectra were recorded on a UV-1800 Shimazdu spectrophotometer in the range of 200–400 nm with a sampling interval of 0.5 nm. The absorption values at a wavelength of 248 nm were used to calculate the rejection values. Analysis of the styrene oligomers was undertaken using an Agilent HPLC system with UV/Vis detector set at a wavelength of 264 nm. Separation was achieved using a reverse phase column (C18–300, 250 × 4.6 mm). The mobile phase consisted of 35 vol% analytical grade water and 65 vol% THF with 0.1 vol% trifluoroacetic acid.[35]

Supporting Information

Supporting Information is available from the Wiley Online Library or from the author.

Acknowledgements

P. Gorgojo and S. Karan contributed equally to this work. The authors wish to acknowledge financial support provided by the 7th Framework Programme of the European Commission's Marie Curie Initiative (NEMOPUR project, grant number 214226–2), EPSRC (ELSEP project, grant number EP/G070172/1), and EPSRC platform grant (EP/J014974/1) entitled Molecular Builders: Constructing Nanoporous Materials.

Received: February 5, 2014
Revised: March 10, 2014
Published online: April 16, 2014

[1] J. L. Humphrey, G. E. Deller, *Separation Process Technology* McGraw-Hill, New York **1997**.
[2] P. Vandezande, L. E. M. Gevers, I. F. J. Vankelecom, *Chem. Soc. Rev.* **2008**, *37*, 365.
[3] I. Soroko, Y. Bhole, A. G. Livingston, *Green Chem.* **2011**, *13*, 162.
[4] Y. H. S. Toh, F. W. Lim, A. G. Livingston, *J. Membr. Sci.* **2007**, *301*, 3.
[5] K. Vanherck, P. Vandezande, S. O. Aldea, I. F. J. Vankelecom, *J. Membr. Sci.* **2008**, *320*, 468.
[6] I. Soroko, A. Livingston, *J. Membr. Sci.* **2009**, *343*, 189.
[7] S. Aerts, A. Vanhulsel, A. Buekenhoudt, H. Weyten, S. Kuypers, H. Chen, M. Bryjak, L. E. M. Gevers, I. F. J. Vankelecom, P. A. Jacobs, *J. Membr. Sci.* **2006**, *275*, 212.

[8] M. F. Jimenez Solomon, Y. Bhole, A. G. Livingston, *J. Membr. Sci.* **2012**, *423–424*, 371.
[9] S. Karan, S. Samitsu, X. S. Peng, K. Kurashima, I. Ichinose, *Science* **2012**, *335*, 444.
[10] D. M. Sullivan, M. L. Bruening, *J. Membr. Sci.* **2005**, *248*, 161.
[11] A. P. Rao, N. V. Desai, R. Rangarajan, *J. Membr. Sci.* **1997**, *124*, 263.
[12] T. M. Murphy, D. S. Langhe, M. Ponting, E. Baer, B. D. Freeman, D. R. Paul, *Polymer* **2011**, *52*, 6117.
[13] S. Sorribas, P. Gorgojo, C. Téllez, J. Coronas, A. G. Livingston, *J. Am. Chem. Soc.* **2013**, *135*, 15201.
[14] P. M. Budd, K. J. Msayib, C. E. Tattershall, B. S. Ghanem, K. J. Reynolds, N. B. McKeown, D. Fritsch, *J. Membr. Sci.* **2005**, *251*, 263.
[15] A. F. Bushell, M. P. Attfield, C. R. Mason, P. M. Budd, Y. Yampolskii, L. Starannikova, A. Rebrov, F. Bazzarelli, P. Bernardo, J. C. Jansen, M. Lanc, K. Friess, V. Shantarovich, V. Gustov, V. Isaeva, *J. Membr. Sci.* **2013**, *427*, 48.
[16] J. Ahn, W.-J. Chung, I. Pinnau, J. Song, N. Du, G. P. Robertson, M. D. Guiver, *J. Membr. Sci.* **2010**, *346*, 280.
[17] P. M. Budd, N. B. McKeown, *Polym. Chem.* **2010**, *1*, 63.
[18] P. M. Budd, E. S. Elabas, B. S. Ghanem, S. Makhseed, N. B. McKeown, K. J. Msayib, C. E. Tattershall, D. Wang, *Adv. Mater.* **2004**, *16*, 456.
[19] S. V. Adymkanov, Y. P. Yampol'skii, A. M. Polyakov, P. M. Budd, K. J. Reynolds, N. B. McKeown, K. J. Msayib, *Polym. Sci., Ser. A* **2008**, *50*, 444.
[20] N. B. McKeown, P. M. Budd, *Chem. Soc. Rev.* **2006**, *35*, 675.
[21] T. Emmler, K. Heinrich, D. Fritsch, P. M. Budd, N. Chaukura, D. Ehlers, K. Ratzke, F. Faupel, *Macromolecules* **2010**, *43*, 6075.
[22] D. Fritsch, P. Merten, K. Heinrich, M. Lazar, M. Priske, *J. Membr. Sci.* **2012**, *401*, 222.
[23] S. Tsarkov, V. Khotimskiy, P. M. Budd, V. Volkov, J. Kukushkina, A. Volkov, *J. Membr. Sci.* **2012**, *423–424*, 65.
[24] N. Du, G. P. Robertson, I. Pinnau, M. D. Guiver, *Macromolecules* **2010**, *43*, 8580.
[25] Q. Song, S. Cao, P. Zavala-Rivera, L. P. Lu, W. Li, Y. Ji, S. A. Al-Muhtaseb, A. K. Cheetham, E. Sivaniah, *Nat. Commun.* **2013**, *4*, 1918.
[26] J. L. Keddie, R. A. L. Jones, R. A. Cory, *Europhys. Lett.* **1994**, *27*, 59.
[27] M. Alcoutlabi, G. B. McKenna, *J. Phys.: Condens. Matter* **2005**, *17*, R461.
[28] J. A. Forrest, K. Dalnoki-Veress, *Adv. Colloid Interface Sci.* **2001**, *94*, 167.
[29] C. M. Stafford, B. D. Vogt, C. Harrison, D. Julthongpiput, R. Huang, *Macromolecules* **2006**, *39*, 5095.
[30] R. A. Riggleman, K. Yoshimoto, J. F. Douglas, J. J. de Pablo, *Phys. Rev. Lett.* **2006**, *97*, 045502.
[31] Y. H. See-Toh, F. C. Ferreira, A. G. Livingston, *J. Membr. Sci.* **2007**, *299*, 236.
[32] Y. Huang, D. R. Paul, *Polymer* **2004**, *45*, 8377.
[33] Y. Huang, D. R. Paul, *Ind. Eng. Chem. Res.* **2007**, *46*, 2342.
[34] T. M. Murphy, D. S. Langhe, M. Ponting, E. Baer, B. D. Freeman, D. R. Paul, *Polymer* **2012**, *53*, 4002.
[35] Y. H. S. Toh, X. X. Loh, K. Li, A. Bismarck, A. G. Livingston, *J. Membr. Sci.* **2007**, *291*, 120.